arXiv:1607.04498v1 [astro-ph.HE] 15 Jul 2016

CHEMICAL AND PHYSICAL PARAMETERS FROM X-RAY HIGH RESOLUTION SPECTRA OF THE GALACTIC NOVA V959 MON

U. Peretz[1], M. Orio[2,3,4], E Behar[1], A. Bianchini[3,5], J. Gallagher[2], T. Rauch[6], B. Tofflemire[2], P. Zemko[5]

[1]Department of Physics, Technion, Haifa, Israel
[2]Department of Astronomy, University of Wisconsin, 475 N. Charter Str., Madison, WI 53706, USA
[3]INAF, Osservatorio Astronomico di Padova, vicolo Osservatorio 5, 35122 Padova, Italy
[5]Dipartimento di Fisica e Astronomia, vicolo Osservatorio 3, Padova University, Italy
[6]Institute for Astronomy and Astrophysics. Kepler Center for Astro and Particle Physics. Eberhard Karls University, Sand. 1., 72076 Tübingen, Germany

[4]marina.orio@oapd.inaf.it

ABSTRACT

Two observations of V959 Mon, done using the *Chandra* X-ray gratings during the late outburst phases (2012 September and December), offer extraordinary insight into the physics and chemistry of this Galactic ONe nova. The X-ray flux was 1.7×10^{-11} erg cm^{-2} s^{-1} and 8.6×10^{-12} erg cm^{-2} s^{-1}, respectively at the two epochs. The first result, coupled with electron density diagnostics and compared with published optical and ultraviolet observations, indicates that most likely in 2012 September the X-rays originated from a very small fraction of the ejecta, concentrated in very dense clumps. We obtained a fairly good fit to the September spectrum with a model of plasma in collisional ionization equilibrium (CIE) with two components; one at a temperature of 0.78 keV, associated with flat-topped and asymmetrical emission lines, blueshifted by $\simeq$710-930 km s^{-1}; the other at a temperature of 4.5 keV, mostly contributing to the high-energy continuum. However, we cannot rule out a range of plasma temperatures between these two extremes; we also modeled the spectrum as a static cooling flow, but the available models and the data quality are not adequate yet to differentiate between the two-component fit and a smoothly varying temperature structure. In December, the central white dwarf (WD) became visible in X-rays. We estimate an effective temperature of $\simeq$680,000 K, consistent with a WD mass $\geq$1.1 M$_\odot$. The WD flux is modulated with the orbital period, indicating high inclination, and two quasi-periodic modulations with hour timescales were also observed. No hot plasma component with temperature above 0.5 keV was observed in December, and the blueshifted component cooled to kT$\simeq$0.45 keV. Additionally, new emission lines due to a much cooler plasma appeared, which were not observed two months earlier. We estimate abundances and yields of elements in the nova wind that cannot be measured in the optical spectra and confirm the high Ne abundance previously derived for this nova. We also find high abundance of Al, 230 times the solar value, consistently with the prediction that ONe novae contribute to at least 1/3rd of the Galactic yield of ^{26}Al.

Keywords: X-rays: stars, stars: abundances, cataclysmic variables, novae: individual (V959 Mon)

1. INTRODUCTION

Novae eruptions occur because of explosive CNO burning at the bottom of the envelope accreted onto WDs in binary systems. Dredged-up and mixed nuclei of C, N and O act as catalysts accelerating the burning and causing the envelope to expand as the electron degeneracy is lifted. Convection brings beta decaying nuclei to the upper layers, heating the envelope and allowing mass ejection. The outflow eventually occurs, mostly, or only, through a radiation driven wind (see Kelly et al. 2013, and references therein). Each outburst ejects mass into the interstellar medium (ISM), from a few 10^{-7} M$_\odot$ to a few 10^{-4} M$_\odot$, depending on the mass accretion rate and time necessary for the pressure at the bottom of the accreted layer to exceed the gravitational pressure. This pressure is mostly an inverse function of the WD mass (Starrfield et al. 2012; Wolf et al. 2013).

Two types of novae are very important for Galactic chemistry. The first type are primordial novae in low metallicity binaries, that should yield Ti and nucleosynthetic end-points around Cu-Zn (José et al. 2007). The second type are

the more common oxygen-neon novae (ONe), attributed to WDs of oxygen and neon. These novae inject a significant amount of dredged up Ne and Mg and many intermediate elements including Al, Ar, Cl, and F into the ISM. Despite the rarity of ONe WDs, if these WDs accrete H-rich material, the outbursts are frequently repeated: there are probably $\approx$15 a year such eruptions in the Galaxy, assuming an observed nova rate of 50 novae of all types each year (see Shafter 1997, 2016). ONe novae play a very interesting role in Galactic chemistry, and we have been able to cast light on their high metallicities with the work we present in this article.

We analyse here in detail two *Chandra* X-ray gratings' observations of the ONe nova V959 Mon, focusing also on the contribution of this nova to the Galactic chemistry. In Section 2 we review the known information about the nova. In Section 3 we describe the observations, and their analysis, including model fits for the ejecta and for the central WDs. Section 4 focuses on the analysis of the ejecta, especially on their chemistry as derived from the "X-ray harder" 2012 September spectrum, with a special attention for the problem of the yield of Al. Section 5 describes the timing analysis of the 2012 December observation. Finally, in Section 6 we discuss our findings and derive conclusions.

2. V959 MON, A NOVA DISCOVERED AS A GAMMA-RAY SOURCE

Nova Mon 2012 (V959 Mon), the best studied ONe nova of recent years, was also the first and only nova detected in gamma-rays before an optical observation. In fact, it exploded when it was angularly close to the Sun and could not be observed at optical wavelengths until August 9, 2012 (Fujikawa et al. 2012). Quite surprisingly, because only two other novae had been observed as gamma ray sources in the two previous years, it was identified with a gamma ray transient discovered with Fermi on June 22, 2012 (Cheung et al. 2012a,b). Unlike the previous two novae discovered as gamma ray sources, Nova Mon 2012 was a slow nova. Greimel et al. (2012) identified the quiescent counterpart, as an Hα luminous, variable source of about 18th magnitude in the r filter. The time t_3 for a decay by 3 magnitudes, a useful quantity to classify novae, is not known. However, because in August of 2012 the spectrum was already nebular, Munari et al. (2013) inferred that t_3 must have been quite shorter than the 45 days since the discovery of the Fermi transient. On the other hand, the light curve decay was smooth and slow after August 2012. The decrease in optical magnitude currently continues, after a slow decline by only about 7 magnitudes in the first 33 months. Munari et al. (2013) noticed that the only change in the rate of optical decline was a break around the time the nova turned off as a supersoft X-ray source, in January 2013 (Page et al. 2013).

The nova is most likely at a distance of about 1.4 kpc (Linford et al. 2015; Munari et al. 2013; Ribeiro et al. 2013) although a larger distance, of 3.6 kpc, has been proposed (Shore et al. 2013). It is effected by a large column density of neutral hydrogen with 5.9-7.4 $\times 10^{21}$ cm^{-2} (measured towards the nova direction according to the HEASARC nH on-line tool, see references therein). Optical spectra of the outburst show many Ne and Mg lines, indicating overabundance of these elements as typical for an outburst on an ONe WD (Munari et al. 2013; Shore et al. 2013; Tarasova 2014). A modulation with a clear period of 7.1 hours was detected in different energy ranges, and it was identified with the orbital period (Munari et al. 2013; Page et al. 2013). The nova was followed at optical and radio wavelengths as it returned to quiescence (Ribeiro et al. 2013). It was recently spatially resolved in the radio (Chomiuk et al. 2014; Linford et al. 2015), revealing that the mass outflow was not symmetric. There was a fast, diffuse bipolar outflow and a dense, slowly moving torus of material in the orbital plane of the binary. Synchrotron emission was detected at the interface between the equatorial and polar regions, which probably was also the origin of the gamma rays in the early post-outburst stage (Chomiuk et al. 2014). The same geometry of the ejecta was clearly inferred also by analysing the optical spectra (Munari et al. 2013; Ribeiro et al. 2013; Shore et al. 2013). Ribeiro et al. (2013) measured a peculiar asymmetric and double-peaked line profile, which they also modeled as a bipolar outflow with expansion velocity reaching a maximum 2400^{+300}_{-200} km s^{-1} at day 130 after the outburst, and inclination $82^o \pm 6^o$. Shore et al. (2013) performed a similar analysis, concluding that the opening angle was of about 70°, at inclination between 60° and 80°. The optical lines observed by the above groups of authors have a broad double peaked profile, which is well pronounced for lines emitted in the outer region of the outflow, but is much less evident for lines originating in the interior region of the ejecta.

The only estimates of abundances in the optical spectra were done by Tarasova (2014), who used the relationship between the spectral line intensities and the ratio of the abundances of ions of N, O, Ne and Ar relative to hydrogen. This author assumed an electron temperature of 10,000 K and with this assumption measured the electron density, $n_e = 10^7$ cm^{-3} in September 25, 2012 and about 1.5 $\times 10^7$ cm^{-3} on October 20 and 24 of 2012, using the forbidden oxygen lines observed in the optical spectra. Later in the outburst, Tarasova found lower values of n_e, 2.4 $\times 10^6$ cm^{-3} and 2.9 $\times 10^6$ cm^{-3} in March 18 and April 17 of 2013, respectively. The value of n_e derived by Shore et al. (2013) using the same method and assuming the same electron temperature was 3 $\times 10^7$ cm^{-3} in November, 2012, so it is seems that there was a rise in the first months, then the shell became diluted at late phases, as mass loss ceased. Tarasova

(2014) measured the abundances of several elements, although with two different methods her results differ by even 50%. The abundances also seem to have changed in time, with a clear increase in Ne. Tarasova (2014) attributed part of this increase to initial clumpiness and inhomogeneity of the shell, making the results less reliable in the first months. However, she attributed most of the increase to a real effect: Ne and O abundances were actually increasing because of the ongoing dredge-up of these elements as the outburst proceeded.

Assuming that the representative abundances for the nova shell should be the ones measured during 2013, when the ejecta homogenized and were better mixed, Tarasova suggested a reliable set of abundances of several elements. Shore et al. (2013) did not measure the abundances, but noticed that the spectra were extremely similar to those of a previous ONe nova, V1974 Cyg, except for Ne, which must have been more abundant in V959 Mon than in V1974 Cyg. Tarasova also estimated that the total ejected mass was about 1.2×10^{-4} $M_\odot$ assuming a distance of 3.6 kpc, but radio imaging done by Linford et al. (2015) implies that the true distance is only 1.4 kpc, reducing this value to $\simeq 1.8 \times 10^{-5}$ $M_\odot$, in perfect agreement with the predictions of recent ONe nova models (Bennett et al. 2013).

V959 Mon was monitored in X-rays with *Swift* and it immediately appeared as an X-ray source since 2012 August 19, but it was not supersoft and luminous until the following month of December. The *Chandra* high resolution spectrum obtained in September showed a bremsstrahlung continuum and many emission lines of several intermediate atomic-number elements. The strongest lines were H-like MgXII at 8.42 Å and Si XIV at 6.18 Å (Ness et al. 2012). This spectrum is particularly interesting because X-ray grating measurements of novae emission lines in the 1.7-10 Å range have been rare, while several atomic transitions that are specific of ONe novae occur in this range. A *Chandra* emission line spectrum was obtained for V382 Vel, a known ONe nova, but only with the LETG grating, which is less sensitive in this range, and at quite a late outburst phase: only Mg lines at $\simeq 8.4$ and $\simeq 9.2$ Å were clearly measurable shortwards of 10 Å (Ness et al. 2005). Two recurrent novae with massive WDs of unknown composition were observed using gratings while they were relatively hard X-ray sources. RS Oph did not show very strong lines of Mg and Al, (Nelson et al. 2008; Ness et al. 2009), consistently with the ultraviolet spectra of a previous outburst (Contini et al. 1995). V745 Sco was observed as a hard X-ray source with NuSTAR (Orio et al. 2015) and shortly later it was observed it with the *Chandra* HETG. Drake et al. (2016) found that the spectrum could be fitted with solar abundances. These two novae host a red giant, thus it is possible that the ejecta were abundantly mixed with the the red giant wind, making it difficult to establish the nature of the secondary. In short, this V959 Mon spectrum is unique, because no other confirmed ONe nova was observed with X-ray gratings when the ejecta, or at least a portion of them, were still so hot to produce the emission lines we measured for this nova. It is very likely, of course, that also other novae underwent a phase in which an X-ray spectrum of emission lines in the 1.7-10 Å range could have been observed and measured, but the X-ray grating observations were not scheduled timely enough. We will show in this paper that the *Chandra* exposures of V959 Mon, and especially this first one, indicate a new avenue to measuring yields of ONe novae.

Once the X-ray spectrum exhibited a supersoft luminous component (Nelson et al. 2012) we proposed a second grating observation in December with *Chandra* and the low energy transmission grating (LETG) coupled with the HRC camera. Initial results, indicating a WD continuum with overimposed emission lines originating in the ejecta, were announced in ATel 4633 (Orio & Tofflemire 2012). In this article we revisit and analyse both *Chandra* observations in detail, focusing especially on the contribution of this nova to the Galactic chemistry.

3. THE OBSERVATIONS

The first X-ray spectrum we analyzed, obtained from the *Chandra* archive tgcat and shown in Fig.1, was taken on September 12, 2012, day 83 of the outburst, with the ACIS-S camera of *Chandra* and the High Energy Transmission Gratings (HETG), following a TOO proposal by Ness et al. (2012). Both the medium energy MEG and the high energy HEG were used, with a respective absolute wavelength accuracy of 0.0006Å and 0.011Å. The exposure time was 25 ks, with a measured count rate 0.18396 ± 0.00280 cts s^{-1} in the zeroth order ACIS-S camera. Half of the incident radiation is dispersed to the gratings in this observation mode, and the count rates were 0.04522 ± 0.00097 cts s^{-1} in the HEG summed first orders (energy range 0.8-10 keV), and 0.08035 ± 0.00129 cts s^{-1} in the MEG summed first orders (0.4-10 keV).

The second observation was proposed by us and carried out on December 03, 2012 (day 165) with the HRC-S camera and the low energy transmission grating (LETG), with wavelength accuracy of 0.04Å (Orio & Tofflemire 2012). The spectrum is shown in Fig. 2. As in the previous observation, the exposure was a little over 25 ks long (25120 seconds). The measured count rate was 0.13648 ± 0.00240 cts s^{-1} with the HRC-s camera, and 0.2103 ± 0.0161 with the LETG summed first orders. There is almost no signal in the HETG spectra longwards of 15 Å, and in the LETG spectrum longwards of 35 Å. We know that *Swift* X-ray telescope observations clearly show that there was no soft X-ray flux in
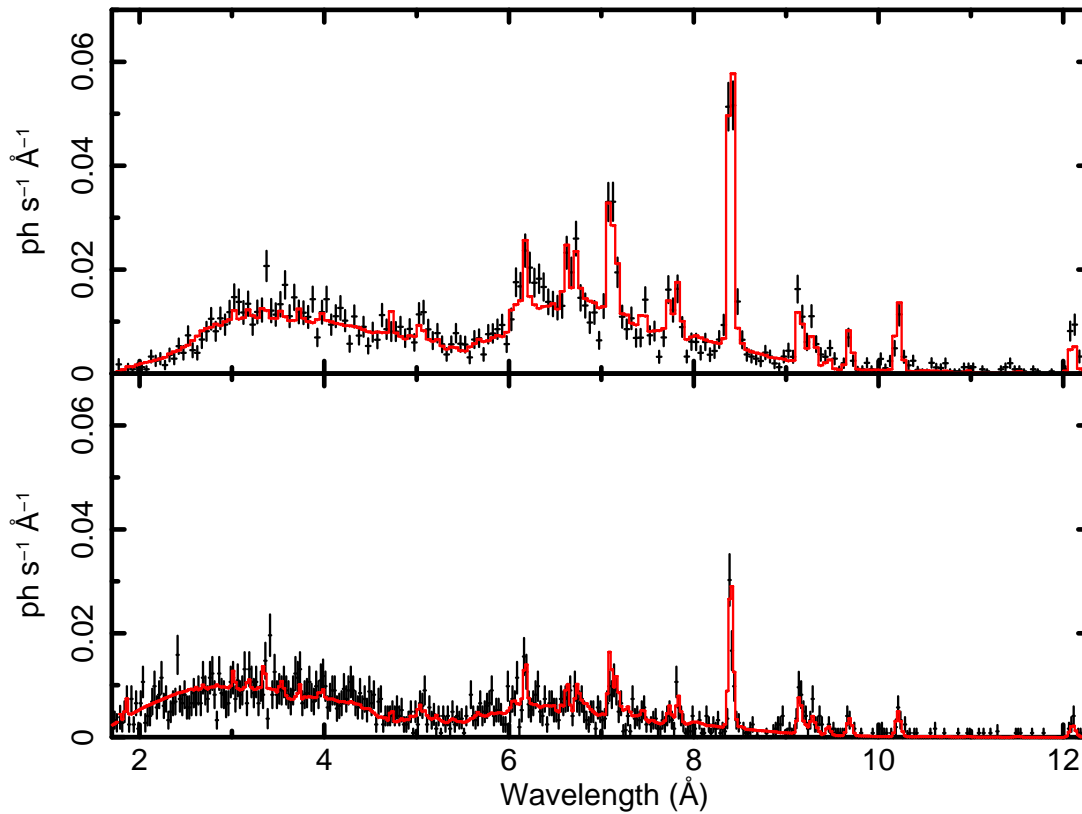
Figure 1. The MEG spectrum (top panel) and the HEG spectrum (lower panel) measured with the *Chandra* HETG on September 12, both binned with 10 counts per bin, and the fit with the model shown in Tables 2 and 3.

September 2012 (Nelson et al. 2012; Page et al. 2013).

3.1. *The spectrum observed in September 2012*

The HETG spectra, shown in Fig. 1, have low signal to noise, but we detect He-like triplets of several elements. In the Si XIII, S XIV, Al XII and Mg XI triplets (the latter shown in Fig. 3) the resonance line appears stronger than the inter-combination and forbidden lines (see Table 1), although the intercombination line is not clearly resolved for Si and S. Depending on the plasma temperature and specific element, the so called G ratio, G=$(f + i)/r$, indicates whether the plasma is in CIE. Generally G>4 indicates a contribution of photoionization (Porquet et al. 2001; Bautista & Kallman 2000), as long as this diagnostic is used in a regime where the forbidden line is not sensitive to the density, that is, extremely high densities. With the method described below, we measured G≃2 for Mg, G≃1.5 for Al, although in the case of Al there was a partial overlap of the f line with a line of Mg XI see Fig. 3. Even taking into account the errors in the measurement, as we see in Fig. 3 the r line is stronger than the other two of the triplet, so the G ratio value is much smaller than a value of 4. These diagnostics points towards a plasma in CIE. The emission lines are blueshifted and broadened, probably because the emission region was extended and not in the collimated bipolar outflows inferred in the optical spectrum . The profile of the lines, shown in Figs. 3 and 4, is asymmetrical and somewhat skewed towards the blue side. Both the blue shift and asymmetry may be due to intrinsic absorption in the nova shell, that erodes the part of the line formed in receding material on the far side. The H-like lines have at least one additional, non-blueshifted component of lower luminosity, due to hotter plasma that can only contribute to the H-like lines because it is almost fully ionized (we will return to this when describing the global fit to the model).

In Table 1 we give the measured fluxes for a few lines that could be relatively well isolated and were measured with good S/N. Since a Gaussian was not a good fit, we examined the spectrum to define the width of the line at the base and the continuum level, and we added all the data points in order to calculate the flux above the continuum. The error
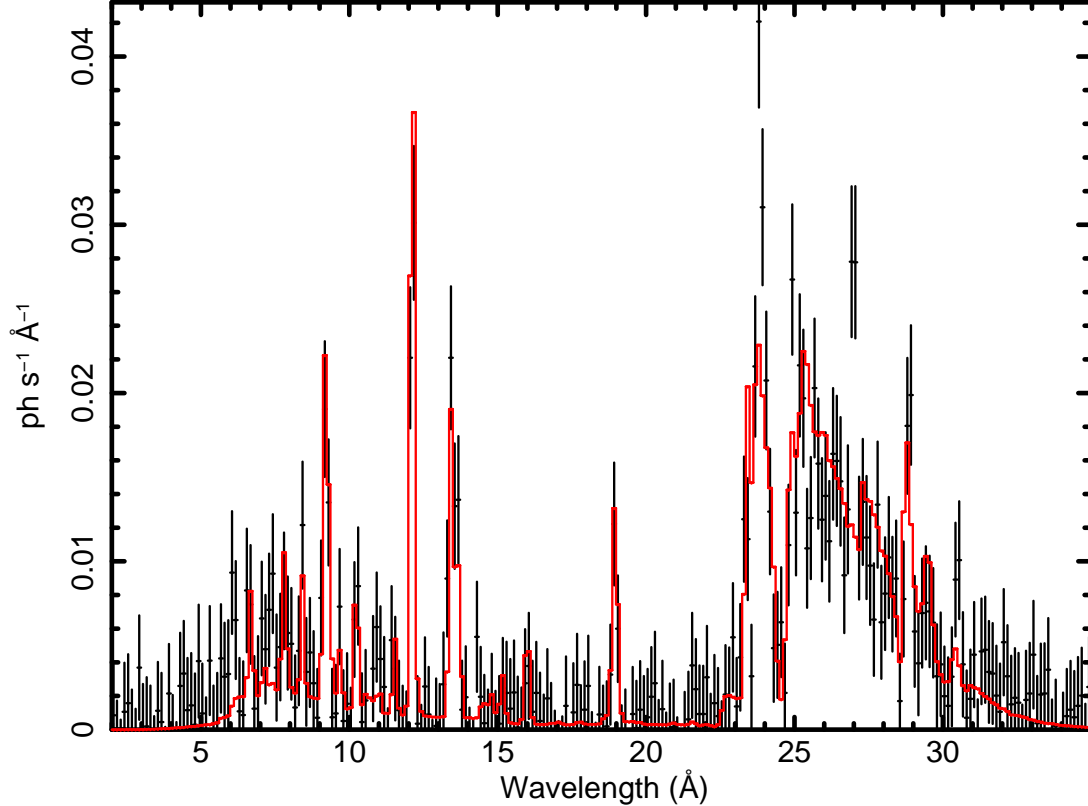
Figure 2. LETG spectrum measured in September of 2012 (in black). For visualizing purposes the spectrum has been binned with 10 counts per bin. The red line shows the fit with the composite model of two thermal plasma components in CIE and an atmospheric model. The parameters of the fit are given in Tables 2 and 3.

on the observed flux was computed as the sum of the squares of the errors of the single data points. The unabsorbed flux (or flux at the source) was calculated by assuming the value of the N(H) derived from a two-component global fit described below, with its additional uncertainty that propagates in the error. In the table we also included the flux of some lines that partially overlap, like the r and i line of Mg XI in Fig. 3, calculated by simply truncating the summatory at the minimum point between the lines (e.g. 0.16 Å in Fig. 3. This introduces an additional error of the order of 10% in the flux calculation for such lines, that is difficult to evaluate exactly and could not be included in Table 1. However, we are mostly interested in flux ratios as diagnostics, and the uncertainty introduced by overlaps in the wings of the lines' profiles does not imply additional uncertainty in the ratios as long as the lines have the same profile, as it is reasonable to assume. especially for lines of the same triplet.

We extracted the spectra with the CIAO software version 4.8.1 and the calibration package CALDB version 4.7.1, then we modeled HEG and MEG spectra simultaneously with the APEC code in XSPEC version 12.9 (Smith et al. 2001); more specifically, we used BVVAPEC. We present the results with errors corresponding to the 90% confidence intervals. Consistently with the profile of the H-like lines and with the excess flux at short wavelengths, we obtained the best fit with two plasma components at different temperatures. A hot component explains the flux at the shorter wavelengths well, short-wards of $\simeq 5$ Å, and a cooler component explains most of the flux in the emission lines. Fig. 4 shows the example of the Mg H-like emission line and how it is fitted with the global model with two components. The cooler plasma component has a much higher flux in the range where most lines are observed. Because no emission lines with significant S/N appear in the lower wavelengths, constraining the velocity of the hot component is not feasible. Depending on the exact parameterization of line widths, the fit converges to either positive or negative velocity. Since the resulting abundances do not depend on this velocity, we present a fit in which we set the hot component velocity to zero. The amount of blueshift due to the cooler component seems to vary for each line, from $\simeq 800$ km s^{-1} to 1250 km

l
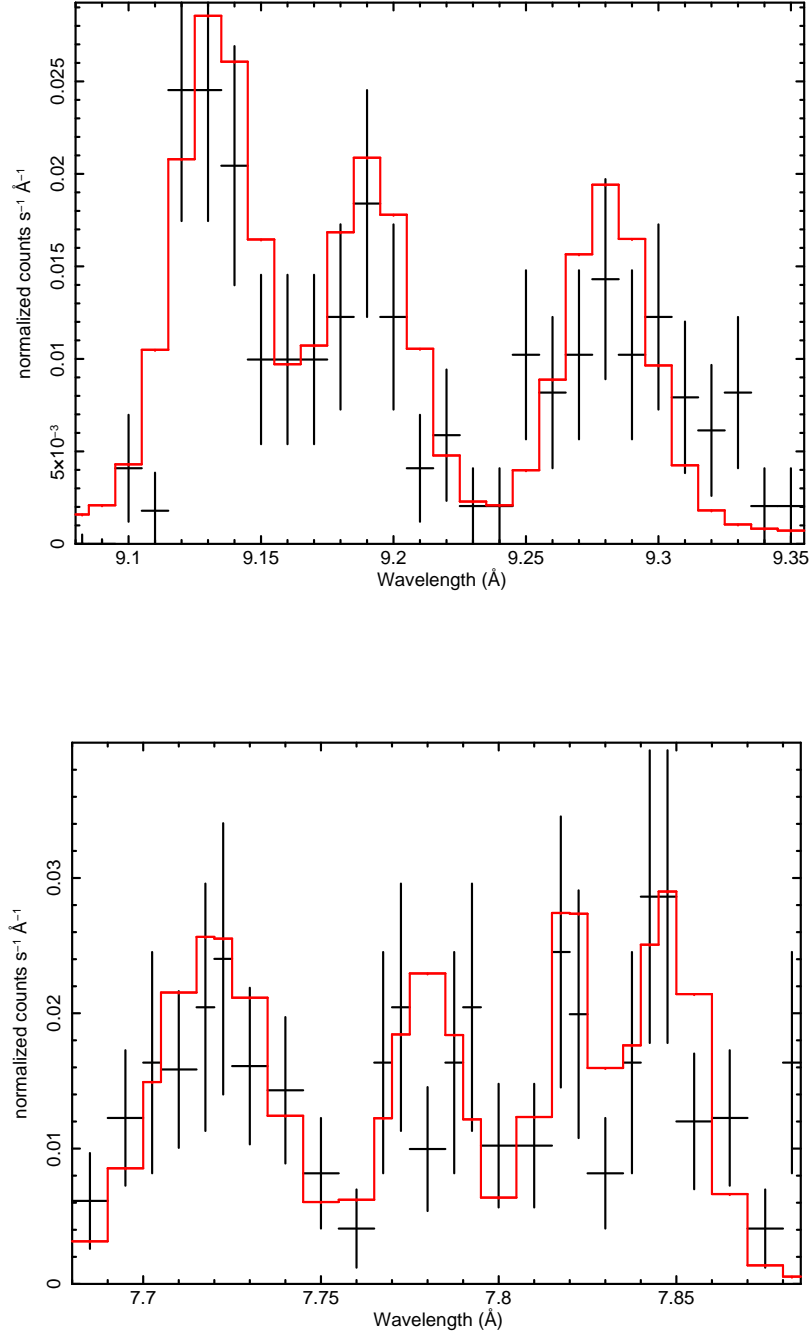
Figure 3. The Mg XI He-like triplet and the Al XII He-like triplet with the Mg XI line at 7.85 Å, measured with the MEG and binned with 2 counts per bin (black data points). Only in order to guide the eye, we traced in red a possible fit with Gaussians having the same width (as calculated also in the "global" model), but slightly different blueshift (however, see text for how the flux in the single lines was computed, without binning and independently of modeling).

s^{-1}, but all are consistent within the 90% confidence level error of the model. In the upper panel of Fig. 4 the same Mg line is plotted in velocity space with the model best fit blueshift marked. In our best fit, the broadening parameter is tied in the two components (for lack of any better constraint), and the lines, which are all clearly broader than the instrumental width, have a fixed velocity at half maximum of 676 km s^{-1}, again visible in Fig. 4. We obtained a good
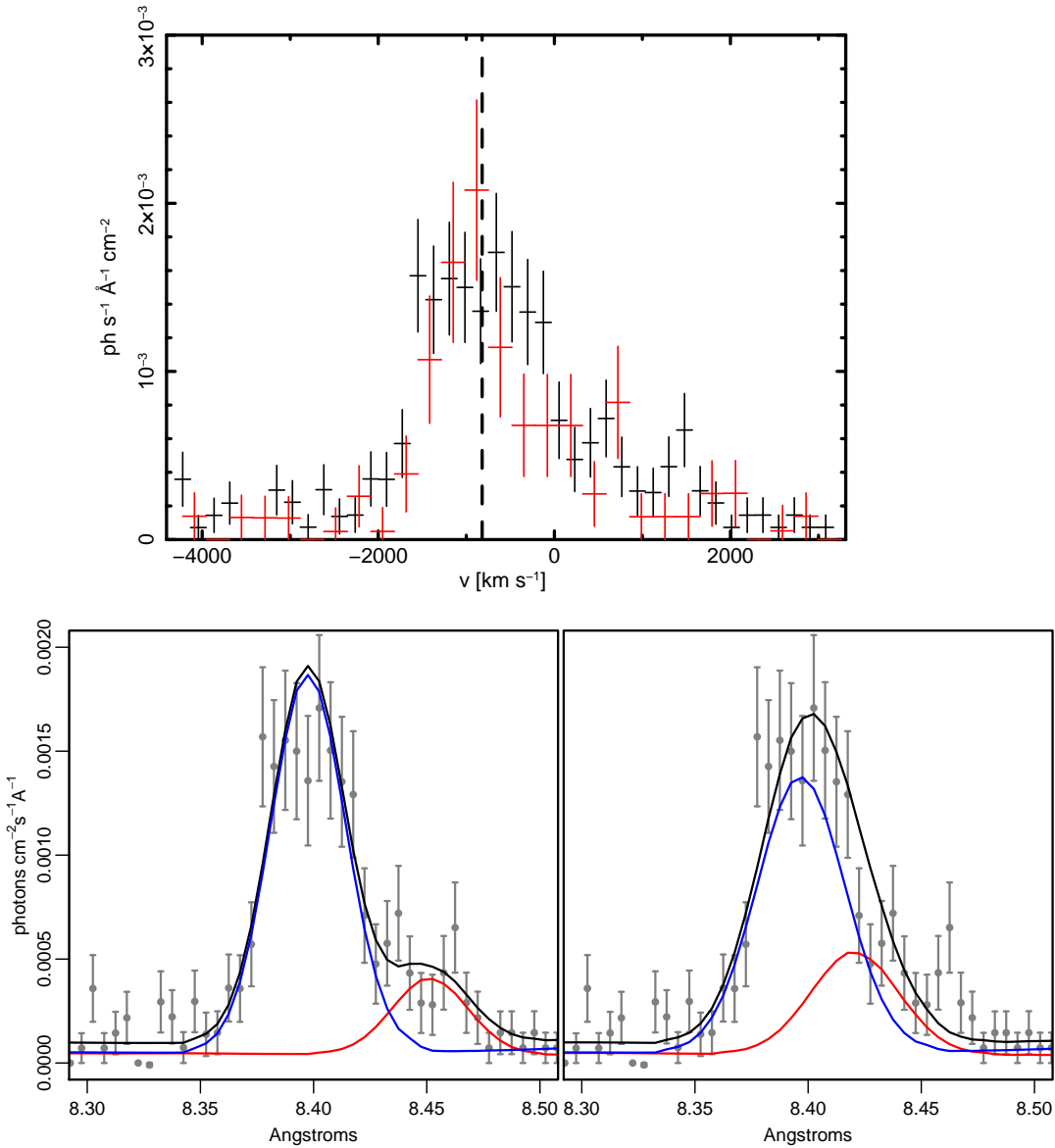
Figure 4. In the top panel the the Mg XII H-like line (an unresolved doublet with contribution of both Lyα_1 λ8.4192 and Lyα_2 λ8.42461) is plotted in velocity space. The MEG data are in black and the HEG ones in red. The dashed line marks the line center of the less hot component, which is clearly blueshifted. The lower right panel shows the same line profile, with the MEG flux as a function of wavelength, as modeled in Table 2: the black solid line is the convolution of the two components of the model, of which the one at 0.78 keV is plotted in blue and the one at 4.5 keV is in red. The right top panel shows the same line and two CIE components model fit, obtained allowing the velocity of the hotter component to vary and resulting in a redshift of the hot component by $\simeq$500 km s^{-1}. This fit is equally statistically significant for the overall spectrum, and the other parameters it returns are only slightly different.

fit constraining also the additional, hotter and non-blueshifted component of the H-like lines to have the same width. Since we used unbinned data for the fit, we used C-statistics (Cash 1979), best suited for fits with a small number of counts per bin, rather than χ^2 statistics. We found a Cstat parameter $c = 5862.51$ and 6346 degrees of freedom.

The model's best fit parameters are in Tables 2 and 3. The best fit negative velocity in the cooler component is -856 km s^{-1} and the lines are broadened by 760 km s^{-1}, much less than the the full width at half maximum (FWHM) measured in the optical emission lines and attributed to the expansion velocity of the two poles by Ribeiro et al. (2013) and Shore et al. (2013), reaching a maximum 3000 km s^{-1}. These groups of authors measure for most emission lines a null center velocity, with equal contribution of blue and red shifted material. First we notice that the flat-topped profile of the less hot component that mostly contributes to the line fluxes is difficult to reconcile with the bipolar

Table 1. Flux of prominent emission lines measured with the MEG. The measurement method is described in the text, and the unabsorbed flux has been evaluated by assuming the value of N(H) of the global models (Table 2). The statistical error does not include the additional error uncertainty due to lines' overlap (however, as discussed in the text, this does not significantly effect the line ratios).).

Ion	Rest wavelength Å	Observed wavelength Å	Absorbed Flux ph cm^{-2} s^{-1} × 10^{-5}	Unabsorbed flux ph cm^{-2} s^{-1} × 10^{-4}
Si XIV	6.180-6.186	6.168	4.915±0.471	3.195±0.345
Al XIII	7.171-7.177	7.155	4.335±0.468	2.819±0.336
Al XII r	7.757	7.720	1.044±0.253	1.061±0.263
Al XII i	7.804-7.807	7.780	0.760±0.210	0.772±0.217
Mg XI	7.850	7.820	0.516±0.166	0.538±0.082
Al XI f	7.872	7.855	0.8320±0.331	0.844±0.338
Mg XII	8.419-8.425	8.380	8.441±0.572	8.576±0.722
Mg XI r	9.169	9.135	2.233±0.402	9.256±1.729
Mg XI i	9.238-9.231	9.190	1.167±0.448	6.731±0.387
Mg XI f	9.314	9.285	2.306±0.577	9.421±0.255
Ne X	10.24	10.210	2.051±0.449	20.51±4.61
Ne X	12.132-12.138	12.105	5.801±0.965	871.10±151.29

Table 2. Parameters in the model fits to the spectra of the HETG (September) and LETG (December) with their 90 % confidence range uncertainties. The abundances are given in Table 3.

Parameter	September	December
General Parameters		
Flux(abs) erg cm^{-2} s^{-1}	$1.7^{+0.1}_{-0.1} \times 10^{-11}$	$8.6^{+0.3}_{-0.3} \times 10^{-12}$
Flux(unabs) erg cm^{-2} s^{-1}	$6.8^{+0.7}_{-0.2} \times 10^{-11}$	$4.1^{+0.6}_{-0.2} \times 10^{-9}$
N(H) ×10^{21} cm^{-2}	32.2^{+5}_{-6}	5.6^{+2}_{-2}
v$_{\text{broadening}}$ (km s^{-1})	676^{+80}_{-70}	1190^{+210}_{-45}
First component		
T$_1$ (keV)	$4.46^{+0.6}_{-0.3}$	$0.071^{+0.03}_{0.03}$
Flux$_1$(abs) erg cm^{-2} s^{-1}	$1.4^{+0.1}_{-0.1} \times 10^{-11}$	$9.4^{+3.0}_{-3.0} \times 10^{-13}$
Flux$_1$(unabs) erg cm^{-2} s^{-1}	$2.9^{+0.2}_{-0.2} \times 10^{-11}$	$4.9^{+2.0}_{-2.0} \times 10^{-10}$
EM$_1$ (10^{54} cm^{-3})	$12.1^{+0.6}_{-0.4}$	$2.3^{+0.5}_{-0.4} \times 10^3$
v$_{\text{blueshift}}$	frozen 0	frozen 0
Second component		
T$_2$ (keV)	$0.78^{+0.4}_{-0.4}$	$0.49^{+0.3}_{-0.3}$
Flux$_2$(abs) erg cm^{-2} s^{-1}	$3.1^{+0.1}_{-0.3} \times 10^{-12}$	$3.1^{+0.3}_{-0.3} \times 10^{-12}$
Flux$_2$(unabs) erg cm^{-2} s^{-1}	$3.9^{+0.1}_{-0.3} \times 10^{-11}$	$1.8^{+0.2}_{-0.2} \times 10^{-11}$
EM$_2$ (10^{54} cm^{-3})	$4.9^{+0.5}_{-0.2}$	$1.6^{+0.2}_{-0.4}$
v$_{\text{blueshift}}$ (km s^{-1})	-856^{+75}_{-145}	-270^{+70}_{-70}
Atmospheric component		
T$_{\text{atm}}$ (K)		$680,000^{+20000}_{-20000}$
v$_{\text{blueshift,atm}}$ (km s^{-1})		2260^{+260}_{-280}
Flux$_{\text{atm}}$(abs) erg cm^{-2} s^{-1}		$4.6^{+0.3}_{-0.3} \times 10^{-12}$
Flux$_{\text{atm}}$(unabs) erg cm^{-2} s^{-1}		$3.5^{+0.2}_{-0.2} \times 10^{-9}$

Table 3. Abundances of the models fitted to the spectra of the HETG (September) and LETG (December). The abundances (relative to solar values Asplund et al. 2006) are assumed equal in the two components of thermal plasma in CIE. The abundances marked with an asterisk were fixed in the fit, as explained in Section 3.

Element	September	December	Optical
He/He$_\odot$	2.5*	2.5*	1.5
C/C$_\odot$	0.9*	0.9*	...
N/N$_\odot$	100*	100^{+160}_{-35}	140
O/O$_\odot$	290*	290^{+160}_{-40}	2.3
Ne/Ne$_\odot$	1660^{+40}_{-160}	190^{+80}_{-120}	40
Mg/Mg$_\odot$	230^{+40}_{-20}	220^{+70}_{-60}	...
Al/Al$_\odot$	250^{+70}_{-70}	770^{+380}_{-380}	...
Si/Si$_\odot$	27^{+5}_{-6}	60^{+40}_{-40}	...
S/S$_\odot$	26^{+15}_{-13}		...
Ar/Ar$_\odot$	37^{+28}_{-32}		0.3
K/K$_\odot$	1340^{+830}_{-830}		...
Ca/Ca$_\odot$	30^{+30}_{-28}	900^{+900}_{-600}	...
Fe/Fe$_\odot$	4^{+5}_{-3}		1.2

outflow inferred from the profile of the optical lines. It seems more likely that in the X-ray emitting material there is "only a modest distortion from spherical", as suggested by Ignace & Brimeyer (2006) for similarly shaped X-ray emission lines of hot stellar winds. Moreover, as already noted above, we cannot rule out that a redshifted portion of the lines may have been completely absorbed, due to optical depth increasing with radius. This effect would shift the apparent peak of the line bluewards and reduce its width (Ignace 2016); the oblique profile towards the red seems to confirm this interpretation. The blueshift of the line center may also be due to the average velocity of the X-ray emitting medium, while the broadening may be caused by the spread of the flow in space; with the present data it is difficult to discriminate between the two cases.

In order to make our assumptions as consistent as possible in each of the two *Chandra* observations and maintain consistency with the optical results as well, we assume that the most abundant elements, He, C, N, and O have the same abundances throughout observations, and that clumping and "late dredge-up effects" did not change abundances significantly while the outburst was still in process and the nova ejecta evolved. Therefore, we fixed the He abundance to match Tarasova's estimates, we assumed an approximately solar C as in many ONe novae (we adopted the value suggested by Shore et al. (2013)), and we fixed the abundances of N and O to match the values we obtained in the fit to the December spectrum, in which prominent emission lines of these elements were measured. The other abundances we derived are presented in Table 3. The relative abundances of the elements with atomic weight larger than oxygen (for example the ratio of Mg or Al to Ne) depend very little on the normalization obtained by fixing the abundances of the less heavy elements, so our assumptions on the H, He, C, O and N abundances for this spectrum are not critical.

We also attempted fitting the data with the cooling flow model VMCFLOW in XSPEC, in order to test the possibility of a smoothly varying temperature as the X-ray emitting plasma travels farther from the WD and cools. We regard this as an experiment, because the cooling flow model in XSPEC does not allow to parameterize the line broadening and to account for different line velocity other than cosmological redshift. Moreover, it includes abundances of fewer elements than the APEC models. The best fit with this model returned a c=6663 value for 7918 degrees of freedom, but only the strength of the most prominent lines is matched, while the continuum was less well fitted than with the apparently more simplistic two component model. This fit returned lower N(H) than the two-component fit, namely 1.71×10^{21} cm^{-2}, a maximum temperature of 4.9 keV and minimum temperature of 100 eV. We note that this lower value is consistent with the suggestion for the *Swift* XRT short observations around the same epoch (Mukai et al. 2014). All the abundances are remarkably lower than in the two-component model, by a factor from 3 to 5, however because no line broadening is included, the line fluxes are significantly underestimated by fitting narrow lines, thus the returned abundances are not reliable. Nevertheless, there are some indications we can derive from this additional modeling for a consistency check. The low minimum temperature in the VMCFLOW model may indicate that the two-component model has underestimated the average temperature of the less hot gas, in which there may be cooler components. For Ne, this may result in largely overestimating the abundance because the peak of emissivity for the strong H-like Ne line is at lower temperature, at 0.54 keV. We will return to this point in Section 4.

The VMCFLOW model is normalized with the rate of in-flowing mass $\dot{m}$, which is a parameter of the model, and corresponds to the mass loss rate for a nova. $\dot{m}$ in the fit turns out to be only 1.2×10^{-8} $M_\odot$ yr^{-1}, two orders of magnitude lower than the estimates by Shore and Tarasova. Constraining $\dot{m}$ a value of 10^{-6} $M_\odot$ yr^{-1} does not result in an adequate fit, but this is not necessarily another shortcoming of this model; in fact we shall discuss in Section 4 that only a small fraction of the outflowing material must be emitting X-rays.

3.2. *The spectrum observed in December 2012: the emergence of the supersoft source*

Tables 2 and 3 show also the parameters of a fit to the LETG spectrum observed in December of 2012 with two plasma in CIE components and a WD atmosphere (Fig. 2). The first important result is the much lower equivalent column of absorbing hydrogen N(H). Because the intrinsic absorption of the ejecta had decreased at this date, N(H) was reduced to 5.6×10^{21} cm^{-2}, which is consistent with the measurement towards the direction of the nova and does not imply intrinsic absorption. It is important to notice that Shore et al. (2013) found that the optical spectrum observed in November of 2012 was consistent with photoionization by a source at about 300,000 K, quite lower than the WD temperature we derive for December. Thus, the emergence of the supersoft source was not only due to the thinning column density, but to actual shrinking of the WD radius at constant bolometric luminosity, while the atmosphere became hotter, as foreseen by all the nova models (e.g. Wolf et al. 2013).

The fit whose parameters are shown in table 2 was done with two CIE plasma components and a hot WD atmosphere. We were not able to obtain a more statistically significant fit adding to the atmospheric model more components at different temperatures, or with the VMCFLOW model. Our proposed 3-component best fit indicates that the hot component seems to have completely disappeared, and that the component in which the blue-shifted lines are produced has cooled from 0.78 keV to 0.49 keV. The line centers in this spectrum are still blueshifted, but by only 270 km s^{-1}. The new, cool component of CIE plasma reaches the XSPEC BVVAPEC model lower limit of $\simeq 70$ eV, and fits the emission lines in the low energy (i.e. supersoft) band. We suggest that these lines are *not* associated with the WD: they are too strong to be attributed to the WD atmosphere (compare with models by Rauch et al. 2010; van Rossum 2012), and consist of different species and ionization potentials than the observable WD absorption features. Superimposed on the WD atmospheric continuum we measure in this spectrum several Ca lines and a strong N line at 29.2 Å. The main purpose of this observation was to measure the temperature of the central, supersoft X-ray source, i.e. the WD. The atmospheric temperature seems to be well constrained at 680,000 K by fitting the supersoft portion of the spectrum with a static model in which the absorption features are blueshifted by 2260 km s^{-1}. The specific model with which we obtained a best fit, chosen in Rauch's model grids described Rauch et al. (2010) and publicly available is the one in the table called SSS_003_00010-00060.bin_0.002_9.00.fits. We note that an alternative blackbody model component did not allow us to obtain a statistically significant fit; we froze the parameters of the BVAPEC components to the values obtained with the atmospheric fit, in order to have fewer parameters to fit, and we obtained a blackbody temperature of 30 eV (360,000 K), but the continuum level was largely overestimated and the fit was much less statistically significant than the one with the atmospheric model.

The blueshift in the absorption features implies that there was be a residual wind, possibly with low mass loss rate, even when the photosphere has receded to a radius close to that before the outburst. It has been pointed out by van Rossum (2012) that in this case the static model only gives an upper limit for the atmospheric temperature, because the flux is still emitted by a larger surface than that of a static WD, although for the nova examined by van Rossum, V4743 Sgr, we find that assuming the same column density N(H) the difference in temperature the static model with appropriate abundances and the wind model is less than 100,000 K. Since no wind-atmospheric model is available for such extremely non-solar abundances as those predicted by the models in the atmosphere of both CO and ONe H-burning WDs (Rauch et al. 2010), we used the static atmosphere model as best approximation. We suggest that the best-fit temperature of the static model, for this spectrum which is observed near supersoft maximum luminosity (see the *Swift*-XRT hardness ratio curve plotted by Page et al. 2013), returns a closely approximated value for the maximum T_{eff}. Even if the static model does not account for the residual small expansion of the atmosphere, it does fit the absorption features well, as it has been noted for other novae as well (see also the case of V2491 Cyg, [Ness et al. 2009). If this is the peak temperature, the T_{eff} indicates a WD mass only slightly larger than 1.1 $M_\odot$ (see Wolf et al. 2013), however we know from Page et al. (2013) that the peak of supersoft emission occurred about 20 days later, so the WD may have later   become hotter. We used also for this fit C-statistics, due to the low counts/bin, and obtained $c = 3194.91$ and 2622 degrees of freedom.

The luminosity of the supersoft component obtained from the fit is too low to originate from the whole WD surface. We find an absorbed flux of 4.6×10^{-12} erg cm^{-2} s^{-1} and an unabsorbed flux of 3.5×10^{-9} erg cm^{-2} s^{-1}, corresponding to a luminosity of 10^{36} erg s^{-1} in the 0.15-1 keV band at 1.4 kpc distance. At the derived atmospheric temperature,

the X-ray luminosity is only about 1.7% of the bolometric luminosity, 6×10^{37} erg s^{-1}, calculated by Wolf et al. (2013) for a WD with the effective temperature returned by the fit. Of course, we are measuring the average flux and luminosity over the whole observation, and as we explain in detail in Section 5, the supersoft flux is modulated with the orbital period. We can thus conclude that on average, during the orbital period only a very small portion of the WD surface is observed. We suggest this may be due to a non-disrupted, or re-formed, accretion disk, because of the high inclination and the consequent orbital modulation. During the orbital period different portions of the WD are visible, but largest portion of the WD surface is obscured by the accretion disk. Section 5 presents the resulting light curve modulation, already observed by Page et al. (2013).

4. THE MASS OF THE X-RAY EMITTING MATERIAL AND THE CHEMICAL YIELDS

The fit is normalized using the emission measure EM$=\int n_e n_i \mathrm{d}V \approx n_e n_i V$, where n_e and n_i are the electron and ion densities and V is the total emitting volume. The mass M of the material in which the X-rays originate is dominated by the ions, $M = Y m_p N$, where m$_p$ is the proton mass and $Y m_p$ is the mean atomic weight of the N ions. In such a metal rich plasma, one cannot consider the mass of hydrogen atoms as representative; in fact Tarasova (2014) found the ejecta to consist of about 53% H and 33% He. We assume here that the chemical composition of the optically-emitting and the X-ray emitting plasma is approximately the same. Moreover, $N = X\ n_H\ V$ or $N = X\ EM/n_e$ where X is the mean proton number, $X = 1.5$ and $Y = 7.5$. The value of Y is dominated by the atomic weight of O (38%) and Ne (30%), with H and He contributing 25%. The mass of the X-ray emitting plasma is

$$M = XY\ m_p\ \frac{EM}{n_e} \approx 11.25\ m_p\ \frac{EM}{n_e} \qquad (1)$$

and is crucially dependent on the value of the electron density n_e.

The most sensitive diagnostic of electron density is the R$=f/i$ line ratio, where f and i are the forbidden and intercombination line fluxes of an He like triplet (Gabriel & Jordan 1969; Porquet et al. 2001). In fact, when this ratio is low, the density is so high that the collisional de-excitation rates are close to the radiative decay rates. When the two rates are comparable, the radiative decay fraction from an excited level is reduced and so the emission becomes weaker. Orio et al. (2013) found that the Ne IX He-like triplet in the U Sco X-ray grating spectra was not consistent with the low density limit. For the September spectrum, the value that we obtain for the Mg He-like triplet measured in Table 1 is R$=1.40\pm0.52$. With R<1.92, the $1\ \sigma$ confidence maximum value, the above authors found an electron density $n_e > 6 \times 10^{10}$ cm^{-3} unless there is a very strong source of photoexcitation. We note that the density is at least of the order of 10^9 cm^{-3} within the $3\ \sigma$ error of the ratio we measured. The effective temperature of the ionizing central source was about 300,000 K two months later (Shore et al. 2013). Even with the WD at this effective temperature (but almost certainly it was still less hot), all the emitting plasma should have been within about 6×10^{10} cm from the WD to undergo photoexcitation. Such a distance is quite interior in the ejecta, but with *Swift* an approximately constant level of X-ray flux was observed since 4 weeks before the HETG exposure. Because we are measuring a velocity of hundreds of km s^{-1}, it is not conceivable that the X-ray emitting plasma is confined in this a small volume.

It thus seems that in September there was not sufficient ultraviolet flux to alter the R value, so high electron density seems to be the likely conclusion (Gabriel & Jordan 1969; Porquet et al. 2001): its value in September must have been indeed high enough to quench the forbidden line.

As mentioned in Section 2, the value of n$_e$ found by Shore and by Tarasova to be consistent with the optical spectra is about 10^7 cm^{-3}. This much higher n$_e$ derived from the X-ray HETG spectrum implies that the X-ray emission comes from a very small fraction of the ejecta, not more than one hundredth the mass of the optically emitting shell; most likely the ejected X-ray emitting material was in very dense clumps. The sum of the emission measures of the two plasma components for the September spectrum is 6.1×10^{55}, implying M$=1.15 \times 10^{33}/n_e$, or that the X-ray emitting mass M was

$$M < 5.75 \times 10^{-10}\ M_\odot \qquad (2)$$

assuming $n_e > 10^9$ cm^{-3}. This is only a small fraction of the mass of $1.8 \times 10^{-5}\ M_\odot$, derived above from Tarasova's work, after correction for the revised distance, for the ejecta emitting at optical wavelengths.

In the December LETG spectrum we do not have density diagnostics to assess whether the emission of the material emitting in CIE conditions was still very dense and clumpy. We do not rule out that the X-ray emitting mass had actually increased, as more mass was ejected, and that the lower X-ray flux is due to a much more diffuse, as opposed to less massive, X-ray emitting material.

For the September HETG spectrum, measured with better signal to noise than the December one because the nova was more luminous at the earlier date in the range of the strongest X-ray emission lines, the line fluxes in Table 1 can

be used for each species to compare the yield in the X-ray emitting material with the abundances predicted by the global model. The global model fit over- or under-estimates the flux of the single emission lines, but gives a statistically significant overall fit. By making assumptions only on two parameters for which the uncertainty is not very large, namely the plasma temperatures and column density derived in the global fit, we found the tabulated emissivities for each line (N(H) must be assumed because the emissivity is based on the unabsorbed flux).

The emissivity of a line emitted at temperature T_e is defined by the following equation:

$$\text{Flux[ph cm}^2\text{ s}^{-1}] = \frac{\epsilon(T_e)Z_\odot}{4\pi d^2} \int n_e n_Z dV \tag{3}$$

where the integral represents the emission measure for a so called "Z" elements, of which n_Z ions are present. $Z_\odot$ is the solar abundance of the given element. The yield of a given ion, Y(Z) is

$$\text{Y(Z)} = \text{m}(Z)\frac{\int n_e n_Z dV}{n_e} \tag{4}$$

where m(Z) is the mass of the single ion, obtained by multiplying its atomic weight by m_p.

We obtained the tabulated values for the emissivity from the ATOMDB database and used the value of the flux to substitute the integral of equation 3 into equation 4. In this way, we calculated the yield of each element divided by n_e, which in turn was divided by equation 1 in order to compute the abundance of the given ion, *independently of n_e* (because this is also a factor in equation 1). We can reasonably assume that most of the elements are in the form of H-like and He-like ions in the plasma at 0.78 keV and in the form of H-like ions for the plasma at 4.5 keV. We found the emissivity of the relevant lines at the given temperatures, and summed the yields obtained from the flux of the H-like and He-like ions (we neglected the latter for Ne). As a first approximation, for the H-like lines we assumed that the mass fraction of the hot and less hot plasma components are given by the ratios of the emissivities computed for the two components in the model fit in Table 1.

With this simple calculation, we obtained an independent check of the abundances of three elements of interest, Ne, Mg and Al. By adding the results of the H-like and He-like r line, as representative of the whole abundance of these elements, we obtained the following values: N/Ne$_\odot$=436±126, Mg/Mg$_\odot$=229±89, Al/Al$_\odot$=170±49 (translating into the following abundances by number: N/Ne$_\odot$=587±169, Mg/Mg$_\odot$=308±146, Al/Al$_\odot$=229±66) (note that here we neglected the error due the uncertainty in the distance). When we compare these values with the values in Table 3, respectively 1660^{+40}_{-160}, 230^{+40}_{-20}, and 250±70, we find a discrepancy for the Ne abundance. The fact that both Al and Mg are consistent with our model indicates the global fit with two components is compensating part of the continuum flux with flux in the Ne line, so that the Ne abundance, while probably high, is lower. For both Ne and Mg abundances, which are very sensitive to the content of plasma at temperature in the 0.3-0.8 keV range, the model's constraints are not very stringent and the uncertainty is still larger than than the statistical uncertainty of the best fit we chose. Because of the low S/N and few counts per bin, a more detailed fitting is not possible with our data, but more accurate determinations of these abundances will be possible in the future for ONe novae observed during the phase of strong emission lines in the range below 20 Å with better S/N. This should be done already with the *Chandra* HETG in new cases of ONe novae effected by lower column density N(H), or larger X-ray emitting mass and total X-ray flux. In the future, *Athena* will make such measurements possible for a majority of ONe novae.

The abundances by number of the most abundant elements ejected in the ISM by other ONe novae, obtained from the analysis of ultraviolet and optical spectra of these novae with the CLOUDY code, are shown in Table 4, together with Tarasova's result for Ne and our results. Despite the still large uncertainties, it seems clear that the X-ray emitting ejecta of V959 Mon were richer in Ne, Mg and Al than the UV-emitting ejecta of other ONe novae. This probably implies a high WD mass; in fact we remind that in the models, the abundances of the elements emitted in the ISM increase with the WD mass, although the same is often not true for their total yield, because the ejected mass decreases with WD mass (in fact the pressure at the base of the envelope to eject mass is reached earlier, see Bennett et al. 2013).

4.1. *The detection of Al lines*

A very important aspect of the X-ray spectra of V959 Mon is the detection of Al lines. The lines of this element have previously been observed only in the ultraviolet spectra of novae. For the September spectrum, we were able to determine that Al/Al$_\odot$ >70, and most likely its value is in the 170-250 range.

A diffuse Galactic gamma-ray emission line at 1809 keV indicates radioactive decay of ^{26}Al into ^{26}Mg, due to a steady amount of 2.7±0.7 M$_\odot$ of this isotope in the Galaxy, explained with ongoing nucleosynthesis (Mahoney
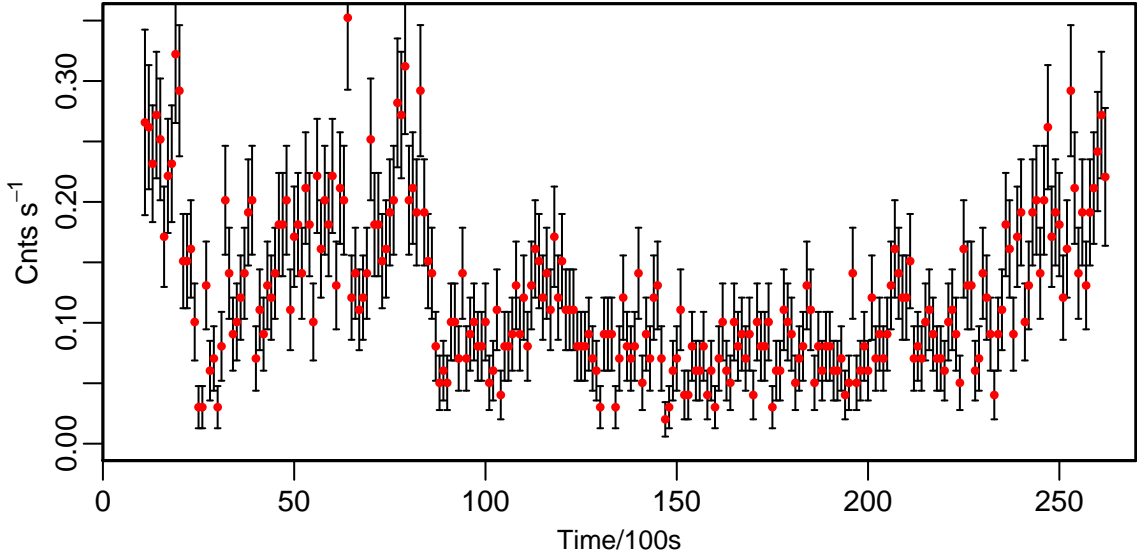
Figure 5. The light curve observed in December of 2012 with the HRC camera, binned every 100 s.

et al. 1982; Diehl et al. 1995). This interesting fact may be very important for the origin of habitable planets, because the radioactive decay of ^{26}Al is the most effective way of heating planetesimal in proto-planetary disks causing differentiation and water sublimation (Srinivasan et al. 1999). In fact, ^{26}Mg is found in meteorites and in presolar dust grains, implying injections of ^{26}Al in the solar system nebula (Hoppe et al. 1994; MacPherson et al. 1995; Huss et al. 1997). There are three astrophysical sites for ^{26}Al nucleosynthesis: the first with most copious production are massive stars; the second, first discovered by Weiss & Truran (1990), are classical and recurrent novae; and the third are asymptotic giant branch stars (see discussion and additional references in Iliadis et al. 2011; Bennett et al. 2013). If the production of novae and asymptotic giant branch stars can be constrained, the rate of production of ^{26}Al can be used to derive the Galactic rate of core collapse supernovae, and with it the production rate of many other elements. By calculating new, relevant reaction rates and ONe novae evolution models, Bennett et al. (2013) recently came to the conclusion that the nova share in ^{26}Al production amounts to 30%.

The fraction of ^{26}Al is expected to be between 11% and 16% of the total yield of Al, and increases with WD mass. Before this work, the abundance of Al has been evaluated using lines in the ultraviolet spectrum, especially Al III λ1860, and Al II λ2669 (e.g. Shore et al. 2003). Also, the Mg abundance can be estimated from the Mg II λ2800 line in the ultraviolet, but it is not measured in optical spectra. We found no flux measurements of Al lines in the literature. Estimating the Al abundance from the ultraviolet spectra is reddening-dependent, model-dependent and has been particularly challenging. In a sample of five novae (see Table 4 and references therein) only three constraining values of Al abundances have been evaluated over the years using UV spectra. The lines appeared to be produced by photoionization by the central source, and the abundances were estimated by line profile fitting performed with the CLOUDY photoionization code (Ferland et al. 2013).

The abundance of Al by mass we obtained for the September observation with the flux method, Al/Al$_\odot$=170$\pm$49 is independent of the value of n_e, although it relies on other parameters obtained from the two component model. If we assume that this abundance is representative of all the ejecta, including the much larger portion that emits only at optical wavelengths (we will discuss this assumption in the Discussion section), and that the total ejected mass was 1.35×10^{-5} M$_\odot$ as referenced above, our result translates into a yield of Al of 1.3×10^{-7} M$_\odot$ injected in the interstellar medium. The mass fraction of Al (^{26}Al+^{27}Al) relative to the solar value in the ejecta is 9.3×10^{-3} (assuming a solar abundance of Al by mass of $5.5 \ 10^{-5}$, or $2.8 \ 10^{-6}$ by number, Asplund et al. 2006). This can be compared with the values predicted by Bennett et al. (2013), 9.5×10^{-3} for a WD of 1.15 M$_\odot$, and 5.1×10^{-3} for a WD of 1.25 M$_\odot$. Bennett et al. (2013) show that, by ejecting mass fractions of Al of this order of magnitude, ONe novae contribute 30% of the galactic yield of ^{26}Al. This result is strongly supported by the present analysis of the V959 Mon X-ray data.
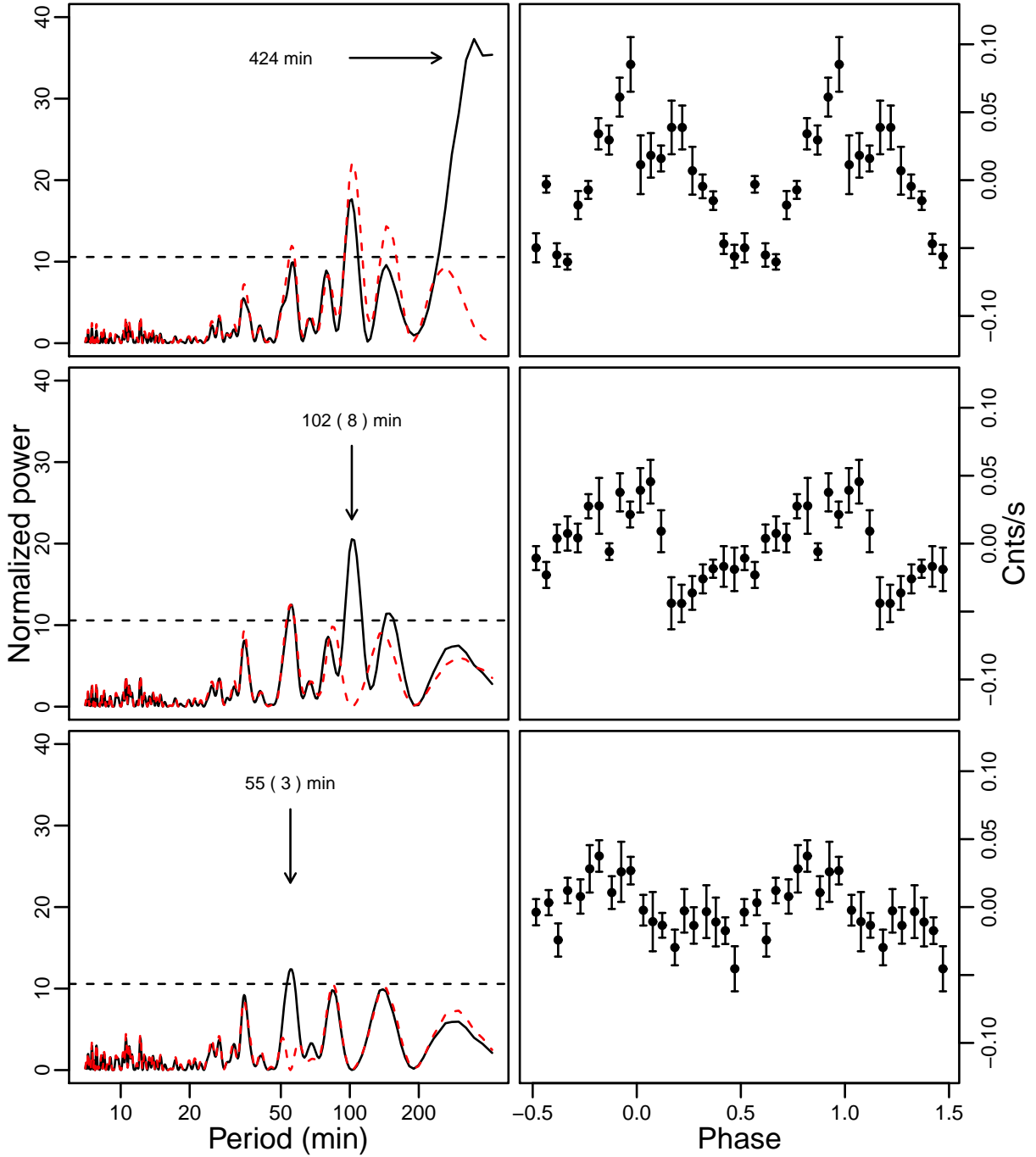
5. TIMING ANALYSIS

Figure 6. The top left panel is the Lomb-Scargle Periodogram (LSP) for the *Chandra* HRC-S zero order light curve observed in December of 2012. The red dashed line shows the LSP after the subtraction of the peak corresponding to the orbital period. The middle left panel shows the LSP subtracting the orbital peak and the red dashed line is the LSP of the data after the subtraction of the 102 min. peak. In the bottom left panel we subtracted the other two modulations and the red dashed line shows the LSP after subtracting the 55 min. period. The panels on the right, from top to bottom show the light curve folded with the orbital, 102 min. and 55 min periods respectively, with the other two modulations subtracted.

While we did not find any significant variability in the September observation, except possibly some stochastic flickering (see also Ness et al. 2012) the supersoft X-ray source observed in December has well defined modulations (see Fig. 5). The 0.295 d (7.08 hrs) modulation reported by Page et al. (2013) is quite prominent in our observation, although the duration of the observation was a little shorter than the period. We tried to subtract the orbital wave using the period reported by Page et al. (2013) and performed the timing analysis with the Lomb-Scargle method. We found several peaks exceeding the height of the 0.3% false alarm probability level (see Fig. 6).

The top left panel is the Lomb-Scargle Periodogram (LSP) for the original data. The red dashed line shows the LSP after the subtraction of the 7.08 hrs (orbital) modulation. The middle panel is the LSP of the data after subtraction of the orbital modulation and the dashed red line is the LSP of the data after the subtraction of the highest peak, of 102 minutes. In the bottom figure we subtracted both the orbital and the 102 min modulation, and show that a 55 minutes period emerged. The 102 and 55 min periods are probably not entirely stable and may be quasi-periodic rather than periodic. The right panels show the phase folded light curves with the relative periods, after the subtraction of the other two modulations: the top right panel is the light curve after the subtraction of the modulations due to the 55 and 102 min periods and folded with the orbital one, the middle left plot is the light curve after the subtraction of the orbital and the 55 minutes modulation, folded with the 102 min period. The bottom panel shows the light curve after subtracting the orbital and 102 min modulation, folded with the 55 min period.

All the periodic modulations are significant at wavelength below 20 Å and are only related to the supersoft component, of which the WD is the main source. Periods or quasi-periods of the order of an hour have already been observed in several novae in the supersoft X-ray source phase (see Orio & Tofflemire 2012; Nelson et al. 2012) and they have been attributed to non-radial g-mode oscillations of the WD.

6. DISCUSSION AND CONCLUSIONS

The *Chandra* spectra of V959 Mon give insight into the nature of the central source and the physical conditions and chemical composition of the ejecta. The observation of the emission lines due to hot ejected plasma in the December 2012 spectrum prompted us to examine the September 2012 archival spectrum. At the earlier epoch, the X-ray high resolution spectrum was still much richer in emission lines due to high ionization potential transitions observed with better S/N than later in December, without superimposition with the WD atmospheric continuum. Both *Chandra* spectra highlight the potential of X-ray high resolution spectra to derive important parameters of the nova physics.

With some assumptions, namely that the optically measured abundances of He and C were the same in the plasma observed in the X-rays, and postulating that the O and N abundances were approximately constant in the two epochs of *Chandra* observations, we were able to estimate absolute abundances of the special elements of which a nova on an ONe WD enriches the interstellar medium. The very large Al abundance of the two-component fit, confirmed by the yield calculation made by evaluating the flux in the H-like and He-like emission lines, implies that ONe novae significantly contribute to the Galactic Al abundance, assuming, of course, that the abundances derived in the small X-ray emitting mass are representative of all the ejecta (there is no reason to think they may be very different). Our results are consistent with the expectations that novae on ONe WDs contribute *at least* 30% of the total galactic yield of Al^{26} in the ISM. Future observations of the spectral region of the Al lines in these novae will clarify the origin of the Galactic Al, a problem that bears implications even in order to evaluate the SN II rate. In the future *Athena* will allow a very accurate estimation of line fluxes in this region for a number of ONe novae.

The lines' ratios in the September spectrum, based on the Mg XI He-like triplet, suggest that the X-rays were emitted by concentration of material of very small total mass (less than 10^{-10} M$_\odot$), concentrated in very small clumps. The spectral shape of the lines suggest a spread in space rather than collimation. The remnant shell of the recurrent nova T Pyx from outbursts previous to 2011 presents a very knotty structure that was flash-ionized again in 2011 (Shara et al. 2015, 1997). Toraskar et al. (2013) attribute these knots to the collision of new ejecta with the swept-up, cold, dense shell from the older outbursts, which would drive Richtmyer-Meshkov instabilities in it. An alternative explanation may be that a fraction of the ejecta, moving more slowly than the rest, is *from the beginning of the outburst* ejected in dense X-ray emitting clumps, which later cool and constitute the clumpy material that was detected by Shara et al. (1997) with HST. This is only a working hypothesis, to be explored in further research, but the concept of small clumps in the ejecta clearly brings to one's mind the image of the old shell of T Pyx.

Williams (2013) attributed hard X-rays to dense blobs of gas colliding with each other while expanding. In this author's scenario, the WD ejecta are all in such blobs or clumps, and they cools very quickly. The more homogeneous circumbinary gas is due instead to mass loss from the secondary. The small mass of X-ray emitting material at a given time would thus depend on the mass loss rate from the WD and the cooling time of the globules. However, for an X-ray emitting mass of the order of 10^{-8} M$_\odot$ and a mass loss rate of the order of 10^{-6} M$_\odot$ year^{-1}, a value that seem reasonable for this nova, the cooling/expanding time must have been of the order of few days, much longer than the minute time scale predicted by Williams (2013). This implies that Williams (2013) model may be viable after carefully revisiting and constraining the physical parameters. Incidentally, we note that, if only a portion of the material is ejected by the WD and a significant part of it is instead ejected by the secondary, this makes difficult to estimate the yield of chemical elements from observations at any wavelengths, so it would be crucial to devise ways to estimate the amount of ejected material from the secondary. The comparison between abundances of the same elements obtained

in the X-ray range and in the optical range may be the best way to obtain this information.

In the September spectrum the emission clearly originated in at least two regions with distinct plasma temperatures, 4.5 and 0.78 keV, both in CIE. However, we could not rule out a smooth variation of temperature between the two values, or a lower minimum plasma temperature. In our best fit model, 57% of the unabsorbed flux (but only 18% of the measured flux) was emitted in blueshifted material that produces slightly asymmetric, flat topped emission lines, probably indicating a large spread in spatial directions and radius-dependent absorption. 43% of the unabsorbed flux (and 82% of the measured, absorbed flux) originated in a much hotter region, contributing to almost a third of the flux in the H-like emission lines. The discrepancy in the evaluation of the Ne abundance obtained with two methods, the global fit and the measurement of the flux in the lines (assuming only the N(H) and emission measure values estimated with the global fit), may imply that the temperature structure is more complex and/or more smoothly varying than our two zones model. In the future, we should study a cooling flow type of model, with gradually changing emissivity, including line broadening and other elements appropriate for the nova physics. In addition to working on the models, we also hope to obtain better quality data for future ONe nova outbursts.

Only one component of plasma in CIE with kT around half a keV was found for the December spectrum, while new emission lines, that most likely are not associated with the central source, had emerged, probably indicating a much cooler plasma (kT≃0.1 keV or less), at the lower limit of the temperature of the CIE plasma models in XSPEC or other analysis packages.

The main goal we had in mind in proposing the December 2012 LETG observation was to measure the WD temperature and chemical composition. It is quite remarkable that the hot WD, emitting supersoft X-rays, emerged and became detectable even at high inclination and with a considerable amount of interstellar absorption towards the nova. The modulation of the central supersoft X-ray source confirms the high inclination at which the system is viewed. This bears implications for those cases in which the central supersoft X-ray source (SSS) is never detected. Ness et al. (2013) have suggested that the detection of the SSS may be impossible in nova system viewed at high inclination, while in these novae the emission line spectrum of the ejecta is better observed and more easily measurable. As a consequence, unless the central source detection is aided by a phenomenon of Thomson scattering (see Orio et al. 2013), we would not be able to draw any conclusion from "missing" SSS (e.g. whether it has not turned on yet, or it has already turned off) because in most systems at high inclination, because the SSS will never appear. Not knowing the range of inclinations, it would be impossible to obtain statistics from the study of extragalactic novae like the one of Henze et al. (2014). The example of V959 Mon, where the SSS eventually was measurable even at high inclination and without clear evidence of Thomson scattering, indicates that a missing SSS is instead more likely to be due to slow evolution in an ejected shell that is optically thick to supersoft X-rays, rather than to the inclination. There are several examples in the literature of novae that in which an emission lines X-ray spectrum later became an SSS X-ray spectrum when the SSS really emerged, like N LMC 2009,(Orio 2013), so we suggest that the inclination is unlikely to be the determining factor in the SSS detection.

We find that the WD temperature was consistent with a WD of at least 1.1 $M_\odot$, comparing our best-fit temperature T_{eff}=680,000 K with the current theoretical models (Wolf et al. 2013). However, the increase in supersoft luminosity in the following two weeks is consistent with a further increase in T_{eff} (Page et al. 2013), probably indicating an even higher mass. In fact, a blueshift of 2260 km s^{-1} in the emission lines indicates residual mass loss, implying that we did not observe the WD after all mass loss had ceased; the WD had not returned to its pre-outburst dimensions yet. However, the detected absorption features are indeed in good agreement with those in the model for a static atmosphere on a WD of mass of at least 1.1 $M_\odot$ (that is, a H-burning WD with peak temperature of, or above, 680,000 K).

The detection of two periods of 55 and 102 minutes respectively in the LETG light curve in 2012 December is consistent with several periodicities measured in the supersoft X-ray source after a nova outburst (Orio & Tofflemire 2012; Ness et al. 2012).

Our final conclusion is that the two *Chandra* grating spectra of V959 Mon highlight the potential of X-ray grating observations to gain insight into the nova physics, by deriving the effective temperature and relative mass of the central WD, by better understanding the dynamics of the mass ejection, and by estimating the chemical yields in the interstellar medium.

REFERENCES

Asplund, M., Grevesse, N., & Jacques Sauval, A. 2006, Nuclear Physics A, 777, 1

Bautista, M. A., & Kallman, T. R. 2000, ApJ, 544, 581

Bennett, M. B., Wrede, C., Chipps, K. A., et al. 2013, Physical Review Letters, 111, 232503

Cash, W. 1979, ApJ, 228, 939

Table 4. Chemical abundances, by number, derived for ONe novae from optical and ultraviolet spectra, compared with the results for V959 Mon.

Nova	Ne/Ne$_\odot$	Mg/Mg$_\odot$	Al/Al$_\odot$	Reference
V382 Vel	17±3	2.6±0.1	21±2	Shore et al. (2003)
QU Vul	21.7 ± 1.7	10 ± 5.1	53.3±14.7	Schwarz (2002)
LMC 1990	62±44	16±7.5	257±98	Vanlandingham et al. (1999)
V693 Cra	247±144	7.9±7	60±59	Vanlandingham et al. (1997)
V838 Her	52.5 ± 2.3	1.4 ± 0.8	29±21	Schwarz et al. (2007)
V1974 Cyg	41.5±17	4.6±3	...	Vanlandingham et al. (2005)
V959 Mon	1660^{+40}_{-160}	230^{+40}_{-20}	230^{+70}_{-70}	2012 September (two-component fit)
	587±169	308±146	229±66	2012 September (flux method)
	190^{+80}_{-120}	220^{+70}_{-60}	770^{+380}_{-380}	2012 December
	95	...	...	2013 March-April Tarasova (2014)

Cheung, C. C., Hays, E., Venters, T., Donato, D., & Corbet, R. H. D. 2012a, The Astronomer's Telegram, 4224, 1

Cheung, C. C., Shore, S. N., De Gennaro Aquino, I., et al. 2012b, The Astronomer's Telegram, 4310, 1

Chomiuk, L., Linford, J. D., Yang, J., et al. 2014, Nature, 514, 339

Contini, M., Orio, M., & Prialnik, D. 1995, MNRAS, 275, 195

Diehl, R., Dupraz, C., Bennett, K., et al. 1995, A&A, 298, 445

Drake, J. J., Delgado, L., Laming, J. M., et al. 2016, ArXiv e-prints, arXiv:1604.04537

Ferland, G. J., Porter, R. L., van Hoof, P. A. M., et al. 2013, RMxAA, 49, 137

Fujikawa, S., Yamaoka, H., & Nakano, S. 2012, Central Bureau Electronic Telegrams, 3202

Gabriel, A. H., & Jordan, C. 1969, MNRAS, 145, 241

Greimel, R., Drew, J., Steeghs, D., & Barlow, M. 2012, The Astronomer's Telegram, 4365, 1

Henze, M., Pietsch, W., Haberl, F., et al. 2014, A&A, 563, A2

Hoppe, P., Amari, S., Zinner, E., Ireland, T., & Lewis, R. S. 1994, ApJ, 430, 870

Huss, G. R., Hutcheon, I. D., & Wasserburg, G. J. 1997, GCA, 61, 5117

Ignace, R. 2016, ArXiv e-prints, arXiv:1601.00552

Ignace, R., & Brimeyer, A. 2006, MNRAS, 371, 343

Iliadis, C., Champagne, A., Chieffi, A., & Limongi, M. 2011, ApJS, 193, 16

José, J., García-Berro, E., Hernanz, M., & Gil-Pons, P. 2007, ApJ, 662, L103

Kelly, K. J., Iliadis, C., Downen, L., José, J., & Champagne, A. 2013, ApJ, 777, 130

Linford, J. D., Ribeiro, V. A. R. M., Chomiuk, L., et al. 2015, ApJ, 805, 136

MacPherson, G. J., Davis, A. M., & Zinner, E. K. 1995, Meteoritics, 30, 365

Mahoney, W. A., Ling, J. C., Jacobson, A. S., & Lingenfelter, R. E. 1982, ApJ, 262, 742

Mukai, K., Nelson, T., Chomiuk, L., et al. 2014, in Astronomical Society of the Pacific Conference Series, Vol. 490, Stellar Novae: Past and Future Decades, ed. P. A. Woudt & V. A. R. M. Ribeiro, 327

Munari, U., Dallaporta, S., Castellani, F., et al. 2013, MNRAS, 435, 771

Nelson, T., Mukai, K., Sokoloski, J., et al. 2012, The Astronomer's Telegram, 4590, 1

Nelson, T., Orio, M., Cassinelli, J. P., et al. 2008, ApJ, 673, 1067

Ness, J.-U., Shore, S. N., Drake, J. J., et al. 2012, The Astronomer's Telegram, 4569, 1

Ness, J.-U., Starrfield, S., Jordan, C., Krautter, J., & Schmitt, J. H. M. M. 2005, MNRAS, 364, 1015

Ness, J.-U., Drake, J. J., Starrfield, S., et al. 2009, AJ, 137, 3414

Ness, J.-U., Osborne, J. P., Henze, M., et al. 2013, A&A, 559, A50

Orio, M. 2013, The Astronomical Review, 8, 71

Orio, M., Rana, V., Page, K. L., Sokoloski, J., & Harrison, F. 2015, MNRAS, 448, L35

Orio, M., & Tofflemire, B. 2012, The Astronomer's Telegram, 4633, 1

Orio, M., Behar, E., Gallagher, J., et al. 2013, MNRAS, 429, 1342

Page, K. L., Osborne, J. P., Wagner, R. M., et al. 2013, ApJ, 768, L26

Porquet, D., Mewe, R., Dubau, J., Raassen, A. J. J., & Kaastra, J. S. 2001, A&A, 376, 1113

Rauch, T., Ringat, E., & Werner, K. 2010, ArXiv e-prints, arXiv:1011.3628

Ribeiro, V. A. R. M., Munari, U., & Valisa, P. 2013, ApJ, 768, 49

Schwarz, G. J. 2002, Apj, 577, 940

Schwarz, G. J., Shore, S. N., Starrfield, S., & Vanlandingham, K. M. 2007, ApJ, 657, 453

Shafter, A. W. 1997, ApJ, 487, 226

—. 2016, ArXiv e-prints, arXiv:1606.02358

Shara, M. M., Zurek, D. R., Williams, R. E., et al. 1997, AJ, 114, 258

Shara, M. M., Zurek, D., Schaefer, B. E., et al. 2015, ApJ, 805, 148

Shore, S. N., De Gennaro Aquino, I., Schwarz, G. J., et al. 2013, A&A, 553, A123

Shore, S. N., Schwarz, G., Bond, H. E., et al. 2003, AJ, 125, 1507

Smith, R. K., Brickhouse, N. S., Liedhal, D. A., & Raymond, J. C. 2001, ApJ, 556, L91

Srinivasan, G., Goswami, J. N., & Bhandari, N. 1999, Science, 284, 1348

Starrfield, S., Timmes, F. X., Iliadis, C., et al. 2012, Baltic Astronomy, 21, 76

Tarasova, T. N. 2014, Astronomy Letters, 40, 309

Toraskar, J., Mac Low, M.-M., Shara, M. M., & Zurek, D. R. 2013, ApJ, 768, 48

van Rossum, D. R. 2012, ApJ, 756, 43

Vanlandingham, K. M., Schwarz, G. J., Shore, S. N., Starrfield, S., & Wagner, R. M. 2005, Apj, 624, 914

Vanlandingham, K. M., Starrfield, S., & Shore, S. N. 1997, MNRAS, 290, 87

Vanlandingham, K. M., Starrfield, S., Shore, S. N., & Sonneborn, G. 1999, MNRAS, 308, 577

Weiss, A., & Truran, J. W. 1990, A&A, 238, 178

Williams, R. 2013, AJ, 146, 55

Wolf, W. M., Bildsten, L., Brooks, J., & Paxton, B. 2013, ApJ, 777, 136

Facilities: Chandra: HETG, ACIS-I, LETG, HRC-S

Software: CIAO, HEASOFT, XSPEC